

# A SMALL X-RAY CORONA OF THE NARROW-ANGLE TAIL RADIO GALAXY NGC 1265 SOARING THROUGH THE PERSEUS CLUSTER

M. SUN, D. JERIUS, & C. JONES

Harvard-Smithsonian Center for Astrophysics, 60 Garden St., Cambridge, MA 02138;

msun@cfa.harvard.edu

Draft version November 18, 2018

## ABSTRACT

A deep *Chandra* observation of NGC 1265 (3C 83.1B), the prototype for the narrow-angled-tailed (NAT) radio galaxy, reveals a small cool X-ray thermal corona ( $\sim 0.6$  keV) embedded in the hot ICM of the Perseus cluster ( $\sim 6.7$  keV). The corona is asymmetric with a sharp edge ( $\sim 2.2''$ , or 0.8 kpc from the nucleus) to the south and an extension to the north (at least  $\sim 8''$  from the nucleus), which is interpreted as the action of ram pressure while solely the static ICM confinement is unable to explain. We estimate that the corona is moving with a velocity of  $\sim 2.4 - 4.2$  times the local sound speed to the south. The presence of the sharp edge for this small corona indicates that the transport processes are largely suppressed by the magnetic field there. The magnetic field around the corona also suppresses heat conduction by at least a factor of  $\sim 60$  across the corona boundary. We conclude that it is unrealistic to study the interaction of the small X-ray coronae with the hot ICM without the consideration of the roles that magnetic field plays, a factor not included in current simulations. An absorbed ( $N_{\text{H}} = 1.5 - 3 \times 10^{22} \text{ cm}^{-2}$ ) nucleus is also detected, which is not usual for FR I radio galaxies. Weak X-ray emission from three inner radio knots in the jets is also detected. Indentations at the east and west of the corona indicate interaction between the jets and the X-ray corona. Narrow jets carry great amounts of energy out of the central AGN and release the energy outside the corona, preserving the tiny and vulnerable corona. This case reveals that the inner kpc core of the corona of massive galaxies can survive both high-speed stripping and powerful AGN feedback. Thus, the cooling of the X-ray coronae potentially provides fuel to the central SMBH in rich environments where the amount of the galactic cold gas is at a minimum.

*Subject headings:* galaxies: clusters: general — galaxies: clusters: individual (Perseus) — magnetic fields — X-rays: galaxies — galaxies: individual (NGC 1265) — galaxies: jets — radio sources: galaxies

## 1. INTRODUCTION

*Chandra* observations have discovered eight small but spatially resolved thermal coronae of early-type galaxies in hot cluster ( $kT_{\text{ICM}} > 3$  keV) environments (Vikhlinin et al. 2001; Yamasaki, Ohashi & Furusho 2002; Sun et al. 2005, S05 hereafter). As summarized in S05, the coronae of massive galaxies can survive in spite of the evaporation and gas stripping by the hot and dense ICM, as well as the energy imparted by the central AGN outbursts. Thus, the properties of these “survivors” can put constraints on important physics, e.g., microscopic transport processes, gas stripping, stellar mass injection and AGN heating (e.g. Vikhlinin et al. 2001; S05). The presence of a dense gas component ( $M_{\text{gas}} \sim 10^8 M_{\odot}$  with a high central density of  $0.1 - 0.3 \text{ cm}^{-3}$ ) potentially provides the fuel for the central supermassive black hole (SMBH), in environments where the amount of the galactic cold gas is at a minimum. Moreover, their properties shed light on the evolution history of their hosts.

For the previous galaxy coronae discovered in rich clusters, there is no strong evidence for a high velocity of the host galaxy relative to the surrounding ICM or for a strong nuclear activity of the host galaxy. In this paper, we show an extreme example for which the galaxy is known to be moving very fast ( $> 2500$  km/s) through a hot cluster and to host a powerful AGN with strong radio emission. NGC 1265 (3C 83.1B, 4C 41.06) is the prototype of narrow-angled tail (NAT) radio sources (Ryle & Windram 1968). NGC 1265 is in the Perseus cluster, 27' northwest of the cluster center (Fig. 1). Its radial velocity (7536 km/s, Huchra, Vogeley & Geller 1999) is  $\sim 2300$  km/s

higher than that of the Perseus cD galaxy NGC 1275 (5264 km/s, Huchra et al. 1999), indicating a large infalling velocity for NGC 1265. Highly complicated radio morphologies are revealed from 2 cm to 92 cm (Owen, Burns & Rudnick 1978; O’Dea & Owen 1986; Sijbring & de Bruyn 1998). Two narrow east-west radio jets emerge from the nucleus, but are quickly bent towards the north to form two tails, which are further merged 4' north of the nucleus. Radio images at 49 cm and 92 cm (Sijbring & de Bruyn 1998) further reveal a low surface brightness extension of the tail that bends at least three times over an angle of almost  $360^{\circ}$ . The projected total length of the tail is at least 40' (or 0.88 Mpc). This complex morphology was tentatively explained as a result of the galaxy’s infalling orbit and the bulk flow of the ICM gas to the east (Sijbring & de Bruyn 1998). Despite the unique appearance of the galaxy in the radio, optically it is a rather normal elliptical. A small dust lane is revealed by the *HST* image (Fig. 1), which is almost perpendicular to the jet direction and aligned with the galaxy major axis. The galaxy is not a strong X-ray emitter from the *ROSAT* data (Rhee, Burns & Kowalski 1994). We obtained a deep (94 ksec) *Chandra* observation on this galaxy and the X-ray source is fully resolved.

The velocity of the Perseus cluster is 5366 km/s (Struble & Rood 1999). We use a redshift of 0.018, to calculate the luminosity distance of NGC 1265, assuming  $H_0 = 70 \text{ km s}^{-1} \text{ Mpc}^{-1}$ ,  $\Omega_{\text{M}}=0.3$ , and  $\Omega_{\Lambda}=0.7$ . The luminosity distance is 78.4 Mpc and  $1''$  corresponds to 0.366 kpc. We use the Galactic absorption of  $1.46 \times 10^{21} \text{ cm}^{-2}$ , which is consistent with the absorption column derived from the X-ray analysis. The solar photospheric abundance table by Anders & Grevesse (1989) is

used in the spectral fits. Uncertainties quoted are  $1\sigma$ .

## 2. *Chandra* OBSERVATION

### 2.1. *Chandra* data reduction

A 93.9 ksec *Chandra* observation was performed with the Advanced CCD Imaging Spectrometer (ACIS) on March 15-16, 2003. The optical axis lies on the CCD S3 and the data were telemetered in Very Faint mode. Standard data analysis is performed which includes the correction for the slow gain change<sup>1</sup>. Since the CCD S1 is off, we investigated the background light curve from the source-free region on the CCD S3. Excluding time intervals with significant background flares results in a total exposure of 65.7 ksec. Although the cluster emission is still significant across the whole *Chandra* field, any weak background flares do not affect our analysis on small scales, since a local background is used. For the analysis of the cluster diffuse emission, we used the period D background file, “aciss\_D\_7\_bg\_evt\_271103.fits”<sup>2</sup>. The particle background level (measured in PHA channels 2500-3000 ADU) was 1.1% higher than that of the period D background data. Thus, we increased the background normalization by 1.1%.

We corrected for the ACIS low energy quantum efficiency (QE) degradation, which increases with time and is positionally dependent<sup>3</sup>. The calibration files used correspond to *Chandra* Calibration Database 3.0.0 from the *Chandra* X-ray Center. In the spectral analysis, a low energy limit of 0.5 keV is used to minimize the calibration uncertainties in low energy.

### 2.2. The spatial properties of the NGC 1265 X-ray source

Despite the gigantic extent ( $> 40'$ ) of NGC 1265 in the radio (O’Dea & Owen 1986; Sijbring & de Bruyn 1998), its X-ray extent is tiny ( $\sim 10''$ ), as shown in Fig. 1. The X-ray emission is composed of a central point source and diffuse emission. The central point source is located within  $0.1''$  of the nucleus determined from the *HST* observation (Fig. 1b)<sup>4</sup>. The soft X-ray emission (0.5 - 1.5 keV) is asymmetric, with a sharp edge  $3''$  south of the nucleus and an extension to the north. The asymmetry is quantitatively shown by the 0.5 - 1.5 keV surface brightness profiles (exposure-corrected) along the south, north and east-west sectors (Fig. 2). The sectors are defined in the caption of Fig. 2. The 0.5 - 1.5 keV surface brightness profiles in the east and west differ very little so we combine them. The surface brightness to the south decreases rapidly at  $\sim 2.5''$  and reaches the background level beyond  $\sim 3''$ , while the brightness profile to the north show excess above the local background to at least  $25''$ . This morphology implies the motion of the X-ray source towards the south and the action of ram pressure by the surrounding ICM. The azimuthally averaged profile is flat beyond  $30''$ , which marks the local background level.

The nuclear point source dominates the hard X-ray emission (Fig. 1a). As there is no statistically important difference on the 2 - 6 keV surface brightness profiles in the south and north, only the azimuthally averaged profile is shown (Fig. 2). The point spread function (PSF) of the central point source was derived with the *Chandra* Ray Tracer (ChaRT), assuming the best-fit absorbed powerlaw spectrum derived from the spectral analysis (discussed later in §2.3). Since the X-ray source is only  $7.1''$

from the optical axis of the observation, the PSF is symmetric. In the 0.5 - 1.5 keV band, the PSF size is much smaller than the source size (Fig. 2). In the 2 - 6 keV band, a model with the PSF plus the local background matches the data well within the inner  $\sim 1.6''$ , but under-estimates the observed brightness of  $2'' - 8''$  at a level of  $5.2\sigma$ . This hard X-ray excess is indicative of low mass X-ray binary (LMXB) emission in NGC 1265, which will be discussed next.

We assume that the LMXB light profile follows the stellar light profile which is derived from the *HST* observation. A bright star  $3''$  east of the nucleus distorts the galaxy image and affects the ground photometry of the galaxy. The center of the star is saturated in the HST F702W image, but not in the F673N image. We subtract the star light and derive the light profile of the galaxy. The galaxy contributes 70% of the total light in the F702W image. The stellar type is unknown, so we simply adopt the same percentage for the B band. The total B magnitude of the galaxy measured from the ground is 12.45 mag after extinction correction and K-correction. Thus,  $L_B = 6.9 \times 10^{10} L_\odot$  for NGC 1265. From the  $L_{\text{LMXB}} - L_B$  scaling relation derived by Sarazin, Irwin & Bregman (2001), the expected LMXB light distributions in the 0.5 - 1.5 keV and 2 - 6 keV band are shown in Fig. 2. In the hard band, a model with a central AGN (PSF), local background and LMXB light roughly re-produces the data, but over-estimate the observed emission by  $\sim 15\%$ . In the soft band, the LMXB emission is able to account for the emission beyond  $9''$ , where the surface brightness profile is much flatter than that within  $9''$ . However, as the LMXB light does not blur the southern sharp edge (Fig. 2), the LMXB emission must be discrete and dominated by those brightest binaries. In the following, we constrain the spectral properties of the X-ray source and the gas properties of the corona.

### 2.3. The spectral properties of the NGC 1265 X-ray source

The spectral properties of the NGC 1265 X-ray source were measured. In view of the asymmetry, we extracted the global spectrum from a  $10''$  radius circle centered  $4.6''$  north of the nucleus. The region is chosen to enclose all X-ray emission of NGC 1265 above the local background (Fig. 2), although the X-ray bright region is considerably smaller (Fig. 1). The background spectrum was extracted from the  $17'' - 73''$  annulus centered on the nucleus. We first used a model with two components (POWERLAW + MEKAL). If only Galactic absorption is applied, the fit is acceptable but the nuclear source has an unusually flat spectrum (Table 1). The presence of a dust lane on the *HST* image may imply extra absorption around the central source. Thus, we allowed additional absorption for the POWERLAW component. As shown in Table 1, the fit is much improved and the derived powerlaw index ( $\sim 2.0$ ) is typical for an AGN. An absorbed nucleus is also supported by the flat 0.5 - 1.5 keV surface brightness profile within the central  $1''$  (Fig. 2). In any case, the corona temperature measurement is robust (0.60 - 0.65 keV). However, in this fit, the LMXB emission (not suffering the excess absorption column) cannot be separated from the nuclear emission. To better separate the thermal corona, the central AGN and the LMXB emission, we extracted spectra in two regions, within  $1.6''$  radius of the nucleus (including nearly 90% of the nuclear emission, Fig. 2), and the

<sup>1</sup> <http://cxc.harvard.edu/contrib/alexey/tgain/tgain.html>

<sup>2</sup> <http://cxc.harvard.edu/contrib/maxim/bg/index.html>

<sup>3</sup> [http://cxc.harvard.edu/cal/ACIS/Cal\\_prods/qeDeg/index.html](http://cxc.harvard.edu/cal/ACIS/Cal_prods/qeDeg/index.html)

<sup>4</sup> The *Chandra* astrometry is generally better than  $0.5''$  (<http://cxc.harvard.edu/cal/ASPECT/celmon/>)

global region excluding the central  $1.6''$  ( $1.6'' - 10''$ , but note the different centers). Separate spectral fits were performed as shown in Table 1. For the inner region, we apply a model with a MEKAL plus an absorbed POWERLAW. For the outer region, we apply a model with a MEKAL plus thermal bremsstrahlung emission from LMXB. The background-subtracted spectra are shown in Fig. 3 with the best fits of the two-component model. Abundances cannot be well constrained (particularly the upper bound) and are fixed at the solar value. The spectral fits to both regions give an abundance lower limit of 0.5 solar (90% confidence level). The allowed abundance change and the inclusion of the hard component do not affect the robustness of the temperature measurement.

We derived the deprojected temperature of the inner region (the fifth row in Table 1) with the standard non-parametric ‘‘onion peeling’’ technique). The spectral properties of the  $1.6'' - 3.2''$  annulus, where the X-ray emission is still rather symmetric, were also examined (the sixth row in Table 1). Gas temperature decreases from 0.7 keV at the outskirts to 0.45 keV within the central 0.6 kpc high-density core, implying the action of radiative cooling. As shown in Fig. 2, the central point source also accounts for some emission in the outer region ( $\sim 29\%$ ) and there may be LMXB emission within  $1.6''$  at the level of  $\sim 5\%$ . However, these extra components bring little change to the fits and computed parameters (including luminosities). The best-fit absorption excess for the AGN is  $\sim 2 \times 10^{22} \text{ cm}^{-2}$ . The 2 - 10 keV and bolometric luminosities of the central AGN are  $5.5 \times 10^{40} \text{ ergs s}^{-1}$  and  $3.0 \times 10^{41} \text{ ergs s}^{-1}$  respectively. The 0.5 - 2 keV and bolometric luminosities of the corona are  $3.3 \times 10^{40} \text{ ergs s}^{-1}$  and  $4.8 \times 10^{40} \text{ ergs s}^{-1}$  respectively. The 0.3 - 10 keV luminosity of the  $1.6'' - 10''$  LMXB component is  $1.8 \times 10^{40} \text{ ergs s}^{-1}$ .

We also examined the spectral properties of the north extension. Its spectrum was extracted from the region defined in Table 1. The result confirms that the north extension is from the emission of thermal gas, while the LMXB component only contributes to  $\sim 5\%$  of the 0.5 - 1.5 keV counts there. The soft coronal emission dominates in the 0.5 - 1.5 keV band. Within  $1.6''$  radius, the nuclear emission only contributes to 6% of the total 0.5 - 1.5 keV brightness. Although the LMXB emission may contribute to  $\sim 24\%$  of the total 0.5 - 1.5 keV emission in the  $1.6'' - 10''$  region, the contribution drops to 10% in a smaller region enclosing all soft X-ray bright region (a  $6.5''$  radius circle centered at  $3.2''$  north of the nucleus). Thus, the 0.5 - 1.5 keV surface brightness well delineates the morphology of the soft corona.

#### 2.4. The properties of the surrounding ICM

We need to know the properties of the surrounding ICM to study the corona-ICM interaction. If NGC 1265 is on the plane of the sky ( $27'$  from the cluster center), the electron density of the surrounding ICM is  $5.9 \times 10^{-4} \text{ cm}^{-3}$  from the ROSAT data (Ettori, Fabian & White 1998). If the galaxy is within  $20'$  (or 439 kpc) of the plane of the sky along the line of sight, the ICM density is  $> 4.1 \times 10^{-4} \text{ cm}^{-3}$ . We take a typical ICM electron density of  $5 \times 10^{-4} \text{ cm}^{-3}$  in this work, but keep the uncertainty in mind. The spectrum of the surrounding ICM ( $16'' - 90''$ ) is studied, as well as that of the whole ICM emission on the S3 CCD. The surrounding ICM (projected) is 10 times hotter ( $\sim 6.7 \text{ keV}$ , Table 1) than the small galaxy corona ( $\sim 0.6 \text{ keV}$ ). The Chandra ICM temperature is consistent with the ASCA value for this region (Furusho et al. 2001).

#### 2.5. The gas distribution of the NGC 1265 corona

We want to characterize the gas distribution of the corona in different directions with the derived 0.5 - 1.5 keV surface brightness profiles. The contribution of the nuclear emission to the soft band and the LMXB emission have to be subtracted. The first component is derived from the PSF and the spectral fits in §2.3, while the LMXB component is estimated from the optical light. Both components are small contributions to the total X-ray emission within  $8''$ . The LMXB component in the south sector is not subtracted, as the scaled LMXB light from the optical light largely over-estimates the actual LMXB light beyond  $3''$  in the south. Nevertheless, any LMXB contribution to the bright core within  $2''$  is small. Since the X-ray source is so small, the Chandra PSF has to be considered in the fits. We applied a model composed of a  $\beta$  model + a constant background for profiles in the south, north and east-west, as well as the azimuthally averaged profile. We also tried to put a truncation radius to the  $\beta$  model, especially for the southern profile. The results are shown in Table 2. Without a truncation radius, the fit to the southern profile yields an unphysical  $\beta$  ( $\gtrsim 10$ ), which is thus not shown. The fits to the profiles in the south and north are shown in Fig. 4. The southern profile is clearly truncated at the sharp edge ( $2.2 \pm 0.3''$  south the nucleus) with a large jump of surface brightness across the edge ( $\sim 106$ ), while the truncations in other directions are not significant with a small surface brightness jump of  $< 3 - 5$ . Despite the large uncertainties, gas distributions (assuming the same emissivity) in all directions are consistent with the same one, but with different truncation radii (or no truncation). We also constrain the width of southern edge by smearing the truncated  $\beta$  model with a Gaussian  $\exp(-r^2/2\sigma^2)$ . The best-fit model requires  $\sigma = 0$  and the 95% upper limit of  $\sigma$  is only 0.2 kpc. We can compare the NGC 1265 corona with the two large coronae in A1367 (S05). Both luminous coronae in S05 are largely symmetric and the surface brightness jump across the presumably pressure-confined boundary is at most 4 - 9. Thus, the sharp edge only  $2.2''$  (or 0.81 kpc) south of the NGC 1265's nucleus is certainly unique and cannot be explained by the confinement of the still ICM pressure.

The gas density and mass can be derived from the surface brightness distribution. The best-fit thermal models of inner and outer regions give almost identical emissivity, if the metallicity is chosen the same. For simplicity, we assume a constant metallicity and a constant emissivity for the whole corona. In view of the unsymmetric shape of the NGC 1265 corona, we applied two methods to derive the density profile and the total gas mass. The first is to use the fit to the azimuthally averaged 0.5 - 1.5 keV profile derived above. Assuming a metallicity of 0.5 - 1.5 solar, the central electron density is  $0.28 - 0.48 \text{ cm}^{-3}$ , and the total gas mass is  $3.2 - 5.4 \times 10^7 M_{\odot}$  (within  $r_{\text{cut}}$  of 7.7 kpc). The second method is to assume that the corona is composed of two hemispheres characterized by the surface brightness profiles of the south and the north respectively. Assuming a metallicity of 0.5 - 1.5 solar, the central electron density is  $0.22 - 0.37 \text{ cm}^{-3}$ , and the total gas mass is  $2.4 - 4.2 \times 10^7 M_{\odot}$  (within  $r_{\text{cut}}$ ). Thus, the central electron density of the corona is  $0.22 - 0.48 \text{ cm}^{-3}$  and the total gas mass is  $2.4 - 5.4 \times 10^7 M_{\odot}$ . Assuming a central abundance of 0.5 - 1.5 solar, the central gas cooling time is only 5 - 15 Myr.

With the derived gas density profile, the X-ray ISM - ICM thermal pressure ratios at the southern edge and the northern tail can be estimated. We assume an ISM temperature of  $0.69 \pm 0.04$

keV (Table 1) and applied Monte-carlo simulations to calculate the errors. The derived X-ray ISM - ICM pressure ratios are  $24 \pm 16$  at the southern edge and  $1.8_{-1.6}^{+1.4}$  at the end of the northern tail. Although the errors are large, the values indicate that the static ICM pressure is not enough to produce the southern sharp edge.

### 2.6. X-ray emission from the jets

X-ray emission, at the significance levels of 2.2 - 3.6  $\sigma$ , is found at the positions of three radio inner knots in the jets (E1, E2 and W1 from O’Dea & Owen 1986). A total of  $\sim 28$  counts are collected from these three knots. Assuming a power law spectrum with a photon index of 2.0, the 0.5 - 10 keV luminosities are  $\sim 1.1 \times 10^{39}$  ergs  $s^{-1}$ ,  $6 \times 10^{38}$  ergs  $s^{-1}$  and  $5 \times 10^{38}$  ergs  $s^{-1}$  for E1, E2 and W1 respectively. Recent *Chandra* observations show that X-ray jet is common in galaxies with radio jets (e.g., Worrall, Birkinshaw & Hardcastle 2001; Sambruna et al. 2004). However, this deep observation of NGC 1265 implies that X-ray jet can be very faint in some cases (at least 40 times fainter than the faintest jet in Worrall et al. 2001). We estimate the 1 keV X-ray to 8-GHz radio flux density ratio over the X-ray detected regions of the jet,  $\sim 10^{-8}$ , which is smaller than what is generally found for low-power radio galaxies where the jet X-ray emission is considered as synchrotron emission ( $\sim 10^{-7}$ , see the list in Evans et al. 2005). Non-detection of NGC 1265’s optical jet is also against the synchrotron interpretation.

In spite of the non-detection of the continuous X-ray jets, there are spatial indentations east and west of the corona (Fig. 1a) that are aligned with the radio jets. These features imply the interaction between the narrow jets and the X-ray corona. The widths of the indentations are comparable to the widths of the radio jets.

## 3. DISCUSSION

### 3.1. The X-ray edge & the velocity of NGC 1265

The sharp X-ray edge is a strong indication of the ISM-ICM interaction. The mean free paths of particles near the edge are:  $\lambda_{\text{ICM}} = 27$  kpc,  $\lambda_{\text{ISM}} = 1.5 (n_{e,\text{ISM}}/0.1 \text{ cm}^{-3})^{-1}$  pc,  $\lambda_{\text{ICM} \rightarrow \text{ISM}} = 60 (\lambda_{\text{ISM}}/1.5 \text{ pc})$  pc, and  $\lambda_{\text{ISM} \rightarrow \text{ICM}} = 5.4$  kpc, assuming temperatures of 6.7 keV and 0.7 keV for the ICM and the ISM near the edge respectively. As  $\lambda_{\text{ICM}}$  is much larger than the size of the corona ( $\sim 4$  kpc in diameter), the ICM may not be treated as fluid relative to the corona. Furthermore, as the galaxy with only stars is rather porous and the corona is so small, it is questionable whether a bow shock can be generated ahead of the corona to change the fluid pattern there. A collisionless bow shock may still be generated as implied by the weak 92 cm emission detected ahead of the X-ray edge (Sijbring & de Bruyn 1998), but this depends on the magnetic field structure around the corona. The magneto-hydrodynamic (MHD) interaction between the galactic magnetic field and the ICM particles (and the magnetic field frozen into them) is however poorly understood.  $\lambda_{\text{ISM} \rightarrow \text{ICM}}$  derived above is much larger than the width of the edge ( $< 0.2$  kpc), which can only be understood if the actual mean free paths of particles are largely suppressed by the magnetic field at the ICM-ISM boundary. Recent simulations of gas stripping and the evolution of X-ray coronae in clusters (e.g., Toniazzo & Schindler 2003; Acreman et al. 2003) tried to study the problem with only fluid dynamics, but did not address the small sizes of X-ray coronae, nor the inclusion of MHD. The observed properties of the NGC 1265 corona demonstrate that

it is necessary to include magnetic fields, especially for small coronae moving in the hot clusters as the mean free path of particles is sensitive to temperature ( $\propto T^2/n$ ).

Our knowledge of the magnetic field in elliptical galaxies is poor (reviewed by Widrow 2002). Moss & Shukurov (1996) proposed two types of seed fields in elliptical galaxies: stellar magnetic field ejected by SNe and stellar winds, and magnetic remnants that arise if elliptical galaxy forms from mergers of spirals. These seed fields have to be amplified by dynamos. They proposed two types of dynamos: acoustic turbulence driven by SNIa and stellar winds, and vortical turbulence driven by stellar motion. Since the magnetic Reynolds number is large, the amplified magnetic field should be frozen in the gas (or the hot gas in elliptical galaxies). When the galaxy falls into the dense ICM, the galactic magnetic field may be compressed and stretched at the boundary, responsible for the suppression of transport processes. However, this simple picture may be too naive as there are a lot of details unclear. Moreover, the small corona of NGC 1265 is surrounded by the hot ICM filling the NGC 1265 galaxy. How the field within the corona can be magnetically isolated from the field in the surroundings (still in the galaxy) is unclear, especially if the turbulent diffusion of magnetic field is important (e.g., Lesch & Bender 1990).

Assuming the radial velocity difference of NGC 1265 and the Perseus cluster is NGC 1265’s radial velocity relative to the cluster, the velocity of NGC 1265 ( $v_{\text{gal}}$ ) is  $2170/\cos\theta$  km/s, where  $\theta$  (between 0 and 90 degree) is the angle between the line of sight and the opposite of the moving direction. The radial velocity dispersion of the Perseus cluster is 1324 km/s (Struble & Rood 1999), which corresponds to a 3D velocity dispersion of 2293 km/s ( $\sigma$ ). NGC 1265’s velocity cannot be too high (e.g.,  $3\sigma$ , or 6880 km/s,  $\theta = 71^\circ 6'$ ) for the galaxy to remain bound.

The sharpness of the X-ray edge implies that  $\theta$  is not small. Otherwise, the edge will be smeared by projection. In principle, we can use the sharp X-ray edge to constrain the velocity of the galaxy. This first requires a good understanding of projection. We performed a number of simulations. The shape of the corona is assumed to be prolate with the nucleus at the center. Since the front of the corona is ablated and compressed by ram pressure, the front is approximated by a large sphere cut by the prolate ellipsoid, while the center of the sphere lies north of the nucleus. The small corona is assumed to be axially symmetric to the direction of the motion. The coronal density profile is represented by a  $\beta$  model with a truncation at the boundary of the corona (see §2.5). The projected morphology of the simulated corona matches the observed morphology well. We compare the projected profiles with the observed ones and find that the X-ray sharp edge cannot be preserved for  $\theta < 45^\circ$ . As  $\theta$  decreases from  $90^\circ$ , the front edge has to be shifted towards the nucleus to allow the projected edge to match the observation. Thus, the best-fit velocity increases as  $\theta$  decreases, opposite from the dependence of velocity on  $\theta$  from the radial velocity constraint. Therefore, the velocity can be in principle constrained well by these two methods. However, several uncertainties prevent a tight constraint on the velocity. First, there is a degeneracy between the ICM density and the galaxy velocity. Second, the coronal density can vary 70% for an abundance change of 0.5 - 1.5 solar. Lastly, the MHD properties of the ICM are not known. For an ambient density of  $5 \times 10^{-4} \text{ cm}^{-3}$ , the best-fit angle is  $50^\circ - 65^\circ$  and the velocity is 3500 - 5000 km/s if we treat the ICM as fluid. Two interesting facts are: 1) the surrounding ICM density is  $> 2 \times 10^{-4} \text{ cm}^{-3}$  if NGC 1265’s

velocity is  $< 5000$  km/s and the abundance of the corona is  $< 1.2$  solar; 2) the abundance of the corona has to be  $< 3$  solar (a tighter upper limit than that derived from the spectral analysis) for the ISM gas to be dense enough to withstand the ram pressure. Combining these constraints, we conclude (conservatively):  $45^\circ < \theta < 67^\circ$  and  $3100$  km/s  $< v_{\text{gal}} < 5500$  km/s (note the local sound speed is  $1.3 \times 10^3$  km/s).

### 3.2. The evolution of the NGC 1265 corona

As the corona moves through the ICM with  $v_{\text{gal}}$  of  $> 3100$  km/s, it is subject to ram pressure stripping and other stripping processes by the surrounding ICM (e.g., Nulsen 1982). The analysis of ram pressure stripping in S05 ignores the high ISM pressure. The survival of NGC 1265's corona in the face of high speed ram pressure stripping and the presence of a sharp edge indicate that high thermal pressure of the inner cooling core is the key to preserve the corona from ram pressure stripping, although the outskirts of the corona are very vulnerable to stripping.

As was discussed in the last section, the physics around the small corona should be best described by MHD. The Kelvin-Helmholtz (K-H) instability may or may not be suppressed. Lacking a good understanding of the relevant physics, only a qualitative discussion is presented. No matter how we treat the surrounding ICM, as fluid or as particles, the typical mass-loss rate of the corona by K-H instability or by the bombardment of the ICM particles is approximately (e.g., Nulsen 1982):

$$\begin{aligned} \dot{M}_{\text{strip}} &\approx \pi r^2 \rho_{\text{ICM}} v_{\text{gal}} \\ &= 0.64 \left( \frac{n_{\text{e,ICM}}}{5 \times 10^{-4} \text{cm}^{-3}} \right) \left( \frac{r}{2 \text{kpc}} \right)^2 \left( \frac{v_{\text{gal}}}{3500 \text{km/s}} \right) M_{\odot} / \text{yr} \quad (1) \end{aligned}$$

This process acts at the boundary of the corona. We calculate the stellar mass injection rate in these two regions,  $< 1.6''$  and  $1.6'' - 10''$ . Using the generally adopted mass injection rate  $\dot{M}_{*} = 0.15 M_{\odot} \text{ yr}^{-1} 10^{10} L_{\odot}^{-1}$  (Faber & Gallagher 1976) and the optical luminosity in the chosen region (from the *HST* data), we estimate  $0.04 M_{\odot} / \text{yr}$  and  $0.15 M_{\odot} / \text{yr}$  for the inner and outer region respectively. The mass deposition rate by cooling,  $\dot{M} \approx 2 \mu m_p L_{\text{X,bol}} / 5kT$ , is calculated in each region to be  $0.19 M_{\odot} / \text{yr}$  and  $0.16 M_{\odot} / \text{yr}$ . Thus, in the inner region, the mass deposition rate is higher than the expected stellar mass injection rate, while in the outer region, the expected mass loss rate by stripping is comparable (if not higher, because of the uncertainties of equation 1) to the expected stellar mass injection rate. Although the mass loss by stripping decreases rapidly to be  $\lesssim$  the stellar injection at radius  $< 1 - 1.6''$ , the cooling rate changes little, if there is no feedback on this small scale. The estimated life time of the current corona is then only 0.1 - 0.2 Gyr.

There are several factors that can reduce the effects of stripping and offset cooling to help the corona to survive much longer. First, the stripping by transport processes can be suppressed by magnetic field. Second, stellar mass injection is a key (e.g., shown in the simulations by Acreman et al. 2003). While the Faber & Gallagher (1976) result is an average, the host galaxies with surviving coronae may have systematically larger stellar mass injection rates than the average. Stellar mass injection outside the corona can also affect the ICM flow pattern there, although the injected ISM gas is not likely to sink into the corona before being stripped and mixed with the ICM. For NGC 1265, if we compare the mass flow rate of the ICM and the expected stellar mass injection rate outside the corona

upstream, on the cross-section of the corona, the latter is only  $\sim 10\%$  of the ICM mass flux, and is not likely to be a significant factor. However, combined with the galactic potential, magnetic field and stellar motion, the ICM flow inside the galaxy (but outside the corona) should be much more complicated than the free flow far away from the galaxy. This may significantly affect the stripping rate estimated by Equation 1. Third, SNIa in principle can provide enough heating energy. Using the SN rate estimates from Cappellaro, Evans & Turatto (1999), the SNIa rate within the size of the NGC 1265 corona is  $\sim 0.2 / 100$  yr. Assuming an energy release of  $6 \times 10^{50}$  ergs per SNIa event, the total energy release of SNe Ia is  $3.8 \times 10^{40}$  ergs  $\text{s}^{-1}$ , which is comparable to the X-ray luminosity of the corona. However, it has been long known that most of SN energy does not couple to the hot gas from the observed  $L_{\text{X}} - L_{\text{B}}$  relation of the X-ray coronae of early-type galaxies (e.g., Brown & Bregman 1998). Thus, the question is how SNIa dissipates its kinetic energy into the hot gas. Lastly, Vikhlinin et al. (2001) proposed that largely reduced heat flux from the surrounding ICM can offset cooling inside the corona if the heat conductivity in the corona is close to the Spitzer value.

As shown in Vikhlinin et al. (2001) and S05, the large temperature gradient from the ICM to the ISM implies that heat conduction must be suppressed. Assuming a corona radius of 2 kpc and an ambient density of  $5 \times 10^{-4} \text{cm}^{-3}$ , we estimate for NGC 1265 that heat conduction has to be suppressed by at least a factor of  $\sim 60$  at the ICM-ISM boundary, using the method presented in S05.

We notice that NGC 1265's ISM must be multi-phase inside the small corona, as implied by the presence of the dust lane. Dust with mass  $\lesssim 10^4 - 10^5 M_{\odot}$  was detected in  $\sim 80\%$  of nearby large elliptical galaxies (e.g., van Dokkum & Franx 1995). Dust detection in radio galaxies is  $\sim 2$  times higher than in radio-quiet galaxies, and the dust lane in radio galaxies is usually perpendicular to the radio axis (van Dokkum & Franx 1995), just as is found in NGC 1265. It has been suggested that the central dust in elliptical galaxies is the product of stellar mass loss from red giant stars (Mathews & Brighenti 2003). This scenario links dust with the  $10^7$  K coronal gas (also thought to have a stellar origin), although it is unknown what the cooling product of the hot gas is. Both cold dust and the cooling product of the high-density X-ray gas (related or not) can provide fuel to the SMBH.

### 3.3. The central AGN and the jets

NGC 1265's nucleus is detected in both radio and X-ray (Fig. 1a). The radio observations show that the central radio source is a compact flat-spectrum source ( $< 0.1''$ , Owen et al. 1978), with a total radio luminosity of  $7.3 \times 10^{38}$  ergs  $\text{s}^{-1}$  (10 MHz - 5 GHz). The X-ray nuclear source is absorbed ( $N_{\text{H}} = 1.5 - 3 \times 10^{22} \text{cm}^{-2}$ ) with a 2 - 10 keV luminosity of  $\sim 5.5 \times 10^{40}$  ergs  $\text{s}^{-1}$ . This high amount of absorption is unusual for FR I radio galaxies, as only NGC 4261 (3C 270) has a similar high absorption column in a systematic study of 25 FR I radio galaxies (Donato, Sambruna & Gliozzi 2004). The conclusion of Donato et al. (2004) is that FR I radio galaxies generally lack a standard optically thick torus, but the exception of NGC 1265 implies that its nuclear X-ray emission comes from somewhere close to the nucleus and some optically thick clouds exist between the nucleus and our line of sight.

The central AGN can have significant impacts on the small corona through its jets, especially in outbursts. NGC 1265 is lu-

minous in radio (3C 83.1B), 8.9 Jy at 1.4 GHz. The radio flux index is 0.67 (from NASA/IPAC Extragalactic Database). From 10 MHz to 5 GHz, the total radio luminosity is  $3.7 \times 10^{41}$  ergs  $s^{-1}$ , while the luminosity of the two jets is  $2.6 \times 10^{40}$  ergs  $s^{-1}$  (O’Dea & Owen 1987, distance adjusted to our value). The jet power is known to be much larger than the radio luminosity of the source. The jet power is distributed in relativistic electrons, ions and magnetic field. The power in ions usually dominates. As the jets of NGC 1265 are bent by the ICM ram pressure, the kinetic power of its jets can be estimated (e.g., Jones & Owen 1979). We assume that the jet flow is non-relativistic, while the power of relativistic jets is much larger. From Euler’s equation, we have:  $\rho_j v_j^2 \approx P_{\text{ram}} R / r_j$ , where  $\rho_j$  is the particle density in the jet,  $v_j$  is the velocity of the jet flow,  $r_j$  is the radius of the jet,  $R$  is the radius of curvature of the bent jet, and  $P_{\text{ram}}$  is the ICM ram pressure. The kinetic power of jets is:  $L_K \approx \pi r_j^2 \rho_j v_j^3$ . With the relation from the bending of jets and adopting  $r_j = 1$  kpc,  $R = 12$  kpc (from the radio image),  $v_j = 10^4$  km/s,  $n_{e,\text{ICM}} = 5 \times 10^{-4}$   $\text{cm}^{-3}$  and  $v_{\text{gal}} = 3500$  km/s,  $L_K = 4.3 \times 10^{43}$  ergs  $s^{-1}$ .  $r_j$  could be smaller but  $v_{\text{gal}}$  may be larger. Their product should not change a lot based on the relation from the bending of jets. The energy in magnetic field is only  $\sim 10\% - 25\%$  of  $L_K$  if the minimum pressure magnetic field is adopted (20 - 30  $\mu\text{G}$  from O’Dea & Owen 1987). The AGN has been active for  $> 10^8$  yr from the length of the tail. We estimate that the total jet power over the active phase of the nucleus is at least 1600 times the thermal energy in the current corona. In view of the great vulnerability of the current corona to AGN feedback, we conclude that the jets carry great amount of energy without dissipation through the small corona, as we previously suggested in S05 for weaker radio sources associated with the coronae in NGC 3842 and NGC 4874.

The interaction of jets and X-ray plasma is highly suggestive from the small X-ray indentations  $2.5''$  east and west of the nucleus (Fig. 1). The radio emission of the jets is anti-correlated with the X-ray emission of the corona (Fig. 1), as the radio emission of the jets turn on after they leave the dense corona. The jets may undergo a transition after they leave the dense corona, possibly because of the change in the external pressure. The coronal thermal pressure,  $1.9 \times 10^{-10}$  ( $n_e/0.1 \text{ cm}^{-3}$ ) (kT/0.6 keV) dynes  $\text{cm}^{-2}$ , is larger than the minimum pressure in the inner knots of the jets,  $6.9 \times 10^{-11}$  dynes  $\text{cm}^{-2}$  (O’Dea & Owen 1987), while the ICM thermal pressure is only  $10^{-11}$  dynes  $\text{cm}^{-2}$ . Thus, the ISM thermal pressure may be enough to confine the jets, while the ICM pressure may not. The edge-brightening of the jets from the first knots implies the action of ram-pressure (O’Dea & Owen 1986). The jets are clearly bent by the ICM ram pressure, rather than the pressure gradient in the ISM, as originally suggested by Jones & Owen (1979).

If the dense core of the corona cools, the cooling product may feed the central SMBH. The stellar velocity dispersion of NGC 1265 is unknown. Using the Faber-Jackson relation and  $M_{\text{BH}}-\sigma$  relation (Tremaine et al. 2002), the mass of the SMBH at the nucleus of NGC 1265 is  $\sim 5 \times 10^8 M_{\odot}$ . Assuming this mass and a central gas temperature of 0.45 keV, the Bondi accretion radius of the central SMBH is 36 pc (or  $0.1''$ ) if the surrounding coronal gas has little residual bulk motion relative to the SMBH. The Bondi accretion rate and the accretion luminosity are  $0.0031 M_{\odot}/\text{yr}$  and  $1.8 \times 10^{43}$  ergs  $s^{-1}$  (assuming a radiation efficiency of 0.1) for a central electron density of  $0.3 \text{ cm}^{-3}$ . The Bondi accretion luminosity is known

to largely over-estimate the luminosity of many low luminosity AGN (e.g., Loewenstein et al. 2001). The possible explanations include that the accretion process is radiation inefficient, and other processes (e.g., feedback) reduce the Bondi accretion rate significantly (e.g., Gliozzi, Sambruna & Brandt 2003).

#### 4. CONCLUSION

The main results of this deep observation of the prototype NAT galaxy NGC 1265 are:

1. A small ( $\sim 4$  kpc) and asymmetric thermal corona is detected around the nuclear region of NGC 1265. A sharp edge is found  $2.2''$  (0.8 kpc) south of the nucleus, while a  $\gtrsim 8''$  extension is present to the north. This indicates a high velocity motion of NGC 1265 towards the south on the plane of sky, which is consistent with the long radio tail to the north.

2. The southern edge is very sharp, with a jump of surface brightness of  $\sim 106$  and a width of  $< 0.2$  kpc. As the mean free paths of particles in the ICM (27 kpc) and from the corona to the ICM (5.4 kpc) are much larger than the width of the edge, magnetic field around the edge is required to significantly reduce the particle diffusion. The interaction between the small coronae and the ICM must be studied by MHD.

3. The temperature of the coronal gas decreases from 0.7 keV at the outskirts to 0.45 keV at the center, while the temperature of the surrounding Perseus ICM (projected) is  $\sim 6.7$  keV. The coronal abundance is consistent with solar. The 0.5 - 2 keV luminosity of the corona is  $3.3 \times 10^{40}$  ergs  $s^{-1}$ . The central electron density is  $\sim 0.22 - 0.48 \text{ cm}^{-3}$ , while the total gas mass is  $\sim 4 \times 10^7 M_{\odot}$ .

4. An absorbed ( $N_{\text{H}} = 1.5 - 3 \times 10^{22} \text{ cm}^{-2}$ ) low luminosity X-ray nucleus is detected, with a 2-10 keV luminosity of  $\sim 5.5 \times 10^{40}$ . This amount of high nuclear absorption column is not usual for FR I radio galaxies.

5. Three inner radio knots are detected in X-rays. Indentations east and west of the corona indicate the interaction between jets and hot gas. There is an anti-correlation between the emission of the radio jets and the X-ray corona (Fig. 1). This implies that jets have undergone a transition as they leave the dense corona.

6. The great vulnerability of NGC 1265’s corona to the large power carried by jets from the central SMBH implies that AGN deposit all energy outside the current corona. This also may imply that AGN heating cannot quench the cooling very close to the nucleus (several kpc) in “cooling-flow” clusters.

7. Constraints from the radial velocity and the X-ray edge yield a velocity for NGC 1265 between 3100 and 5500 km/s, and the angle between the tail and the line of sight is  $45^{\circ} - 67^{\circ}$ .

8. If the stripping, cooling and evaporation are not suppressed, the current corona can only survive for 0.1 - 0.2 Gyr. However, enhanced stellar mass injection, suppressed stripping and SNIa heating (if energy coupled to the hot gas) can significantly increase the lifetime of the corona. For survival of NGC 1265’s corona, heat conduction has to be suppressed by at least a factor of  $\sim 60$  at the ICM-ISM interface.

The survival of NGC 1265’s corona from ram pressure stripping implies that coronae of similar or more massive galaxies can survive  $\gtrsim 1000$  km/s stripping in environments like the core of the Coma cluster. A systematic study based on *Chandra* data is underway, which will better understand the evolution of these small corona in rich clusters, including their fates, fueling of the SMBH, interaction with the environment, and the relation with large cooling cores.

We thank Alexey Vikhlinin, Bill Forman & Paul Nulsen for inspiring discussions. We are grateful to C. P. O’Dea and Ylva Pihlstrom for providing us the VLA images of NGC 1265

shown in Fig. 1. We thank the referee for helpful comments. We acknowledge support from the NASA contracts G02-3184X and Smithsonian Institution.

## REFERENCES

- Acreman, D. M., Stevens, I. R., Ponman, T. J., Sakelliou, I. 2003, MNRAS, 341, 1333  
 Anders, E., & Grevesse N. 1989, Geochimica et Cosmochimica Acta, 53, 197  
 Brown, B. A., Bregman, J. N. 1998, ApJ, 495, L75  
 Cappellaro, E., Evans, R., Turatto, M. 1999, A&A, 351, 459  
 Donato, D., Sambruna, R. M., Gliozzi, M. 2004, ApJ, 617, 915  
 Etti, S., Fabian, A. C., White, D. A. 1998, MNRAS, 300, 837  
 Evans, D. A., Hardcastle, M. J., Croston, J. H., Worrall, D. M., Birkinshaw, M. 2005, MNRAS, in press (astro-ph/0502183)  
 Faber, S. & Gallagher, J. 1976, ApJ, 204, 365  
 Furusho, T., Yamasaki, N. Y., Ohashi, T., Shibata, R., Ezawa, H. 2001, ApJ, 561, L165  
 Gliozzi, M., Sambruna, R. M., & Brandt, W. N. 2003, A&A, 408, 949  
 Huchra, J. P., Vogeley, M. S., Geller, M. J. 1999, ApJS, 121, 287  
 Jones, T. W., Owen, F. N. 1979, ApJ, 234, 818  
 Lesch, H., & Bender, R. 1990, A&A, 233, 417  
 Loewenstein, M., Mushotzky, R. F., Angelini, L., Arnaud, K. A., Quataert, E. 2001, ApJ, 555, 21L  
 Mathews, W. G., Brighenti, F. 2003, ApJ, 590, 5L  
 Moss, D., & Shukurov, A. 1996, MNRAS, 279, 229  
 Nulsen, P. E. J. 1982, MNRAS, 198, 1007  
 O’Dea, C. P., & Owen, F. N. 1986, ApJ, 301, 841  
 O’Dea, C. P., & Owen, F. N. 1987, ApJ, 316, 95  
 Owen, F. N., Burn, J. O., Rudnick, L. 1978, ApJ, 226, L119  
 Rhee, G., Burns, J. O., Kowalski, M. P. 1994, AJ, 108, 1137  
 Ryle, M., Windram, M. D. 1968, MNRAS, 138, 1  
 Sambruna, R. M. et al. 2004, ApJ, 608, 698  
 Sarazin, C. L., Irwin, J. A., Bregman, J. N. 2001, ApJ, 556, 533  
 Sijbring, D., & de Bruyn, A. G. 1998, A&A, 331, 901  
 Struble, M. F., & Rood, H. J. 1999, ApJS, 125, 35  
 Sun, M., Vikhlinin, A., Forman, W., Jones, C., Murray, S. S. 2005, ApJ, 619, 169 (S05)  
 Toniazzo, T., & Schindler, S. 2001, MNRAS, 325, 509  
 Tremaine, S. et al. 2002, ApJ, 574, 740  
 van Dokkum, P. G., Franx, M. 1995, AJ, 110, 2027  
 Vikhlinin, A., Markevitch, M., Forman, W., Jones, C. 2001, ApJ, 555, L87  
 Widrow, L. M. 2002, RvMP, 74, 775  
 Worrall, D. M., Birkinshaw, M., Hardcastle, M. J. 2001, MNRAS, 326, 7L  
 Yamasaki, N. Y., Ohashi, T., & Furusho, T. 2002, ApJ, 578, 833

TABLE 1  
SPECTRAL FITS OF THE NGC 1265 X-RAY SOURCE

Region	Thermal gas		AGN		
	T (keV)	Z ( $\odot$ )	$N_{\text{H}}$ ( $10^{22}$ cm $^{-2}$ ) <sup>a</sup>	$\Gamma$	$\chi^2/\text{d.o.f.}$
<10'' (total) <sup>b</sup>	0.62 $^{+0.02}_{-0.03}$	(1.0)	-	0.94 $\pm$ 0.12	76.9/75
	0.63 $^{+0.02}_{-0.03}$	1.2 $^{+4.9}_{-0.6}$	1.3 $\pm$ 0.3	(1.7)	64.1/74
	0.63 $^{+0.03}_{-0.02}$	0.9 $^{+4.0}_{-0.2}$	1.8 $^{+0.9}_{-0.6}$	2.04 $^{+0.32}_{-0.15}$	63.3/73
<1.6'' <sup>c</sup>	0.51 $\pm$ 0.04	(1.0)	2.4 $^{+0.3}_{-0.4}$	1.97 $^{+0.27}_{-0.20}$	34.7/42
<1.6'' (deproj.) <sup>c</sup>	0.45 $^{+0.05}_{-0.03}$	(1.0)	2.4 $^{+0.5}_{-0.7}$	1.98 $^{+0.13}_{-0.20}$	36.1/42
1.6'' – 3.2'' <sup>d</sup>	0.63 $^{+0.05}_{-0.04}$	(1.0)	-	-	23.7/31
1.6'' – 10'' <sup>e</sup>	0.69 $\pm$ 0.04	(1.0)	-	-	36.4/41
North extension <sup>f</sup>	0.76 $^{+0.07}_{-0.08}$	(1.0)	-	-	8.2/16
16'' – 90'' <sup>g</sup>	6.67 $^{+0.68}_{-0.70}$	0.41 $^{+0.41}_{-0.32}$	-	-	102.6/113
S3 CCD <sup>h</sup>	6.41 $\pm$ 0.25	0.48 $^{+0.10}_{-0.09}$	-	-	192.0/143

<sup>a</sup> The excess absorption column (besides the Galactic value of  $1.46 \times 10^{21}$  cm $^{-2}$ ) for the nuclear source

<sup>b</sup> The global spectrum of the NGC 1265 X-ray source, while the center is shifted to 4.6'' north of the nucleus to account for the asymmetric morphology of the corona. The background is from the surroundings (all the same for corona emission; see text).

<sup>c</sup> Centered on the nucleus

<sup>d</sup> The annulus centered on the nucleus. A 8 keV Bremsstrahlung component is included to model the contribution from LMXB.

<sup>e</sup> The global region excluding the central 1.6'' (radius) region. A 8 keV Bremsstrahlung component is included.

<sup>f</sup> The region is defined as the north half of a  $3.5'' \times 8''$  (east-west semi-minor axis  $\times$  north-south semi-major axis) ellipse centered 1.6'' north of the nucleus, excluding the region within 2.6'' radius of the nucleus. A 8 keV Bremsstrahlung component is included.

<sup>g</sup> The surrounding ICM emission, centered on NGC 1265’s nucleus, with the blank sky background excluded

<sup>h</sup> The integrated ICM emission on the S3 CCD field

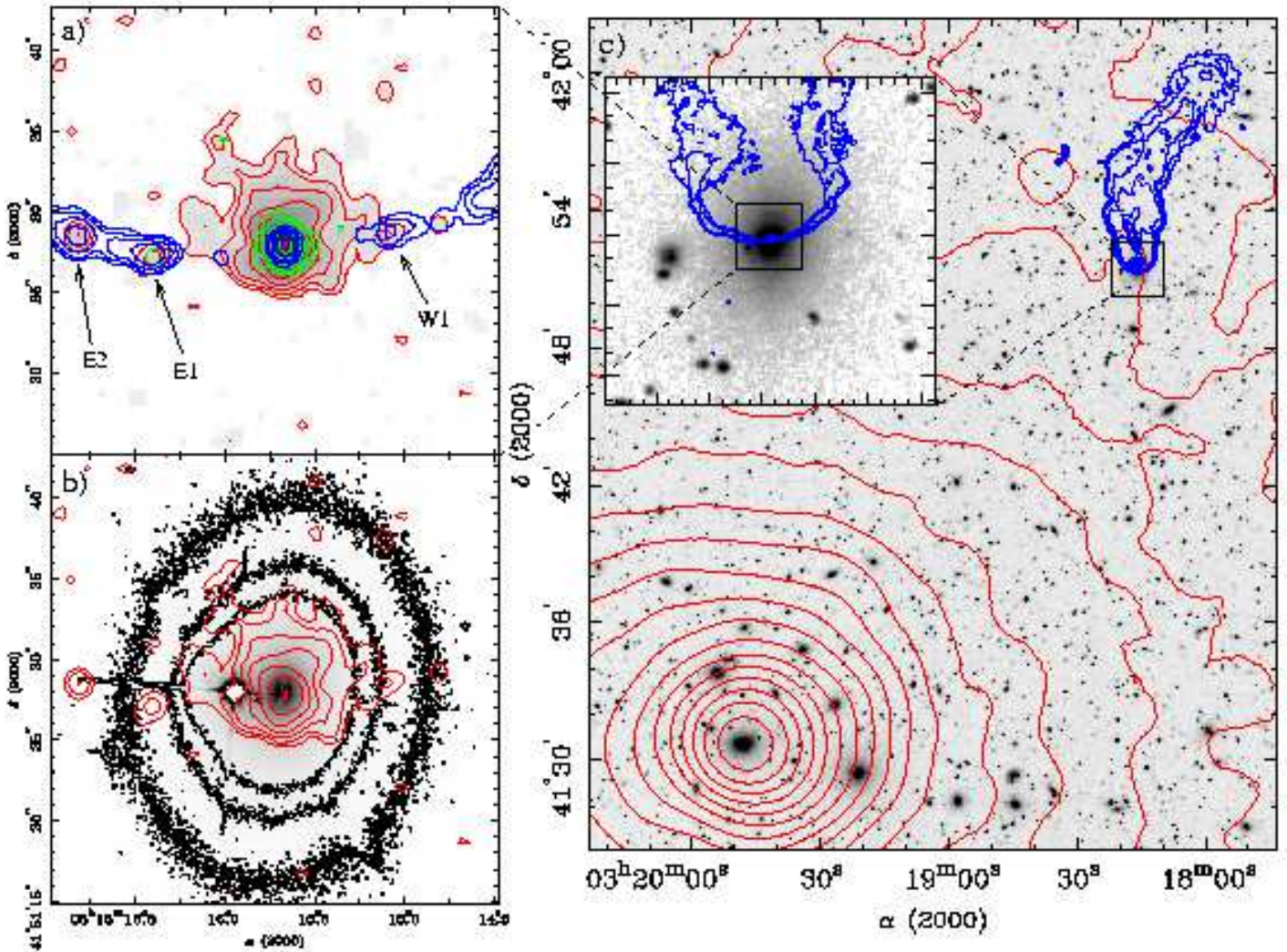


FIG. 1. — a): The 0.5 - 1.5 keV *Chandra* contours (red, from  $0.023$  to  $1.5 \times 10^{-3}$  cts  $s^{-1}$  arcsec $^{-2}$ , separated by a factor of 2) superposed on its own image (exposure corrected, smoothed by one ACIS pixel). The 2 - 6 keV *Chandra* contours (green, from  $0.25$  to  $8 \times 10^{-4}$  cts  $s^{-1}$  arcsec $^{-2}$ , separated by a factor of 2) are also shown (exposure corrected, smoothed by one ACIS pixel). The sharp edge  $\sim 3''$  south of the nucleus is prominent, as well as the extension to the north. A 20 cm VLA image of the jets is shown as blue contours (image from Ylva Pihlstrom,  $1.29'' \times 1.17''$  beam size). The radio jet emission is anti-correlated with the X-ray emission of the corona. X-ray emission from three radio knots E1, E2 and W1 (Fig. 1 of O'Dea & Owen 1986), is also detected. There are indentations in the east and west of the corona along the jet direction, aligned with the knots. This indicates an interaction between the jets and the X-ray gas. b) The 0.5 - 1.5 keV *Chandra* contours superposed on the *HST* WFPC2 image (F702W filter). A dust lane, nearly perpendicular to the jet direction and aligned with the major axis of the galaxy, is detected within the central  $1''$  radius. A nearby bright star ( $\sim 3''$  east of the nucleus) distorts the optical light of the galaxy. The outer contours of the optical light are also plotted. The X-ray light is asymmetric compared to the optical light. c) *ROSAT* contours (red) of the Perseus cluster superposed on the DSS I image. The cluster center (NGC 1275) is on the lower left. A low resolution VLA image of 3C 83.1B (blue contours) is shown (image from Chris O'Dea, Fig. 11 of O'Dea & Owen 1986), with NGC 1265 at the head of the NAT source. The tail of the radio galaxy is at least  $40'$  in projection and bends sharply at least 4 times (see more figures in O'Dea & Owen 1986 and Sijbring & de Bruyn 1998). The region around the galaxy ( $2.3' \times 2.3'$ ) is also enlarged on the left insert, where contours of a 6cm VLA image (from Chris O'Dea) are superposed on the DSS II image. The optical light of NGC 1265 can be traced to the edge of this subfield.

TABLE 2  
THE FITS OF  $S_X$  IN DIFFERENT DIRECTIONS

Direction	$r_c$ (arcsec)	$\beta$	$r_{\text{cut}}$ (arcsec)	$S_X$ jump (@ $r_{\text{cut}}$ )	$f_{\text{back}}$ ( $10^{-6}$ cnts $\text{s}^{-1}$ arcsec $^2$ )	$\chi^2/\text{d.o.f.}$
South	$1.5 \pm 0.5$	$0.66 \pm 0.15$	$2.2 \pm 0.3$	$\sim 106$	$1.90 \pm 0.14$	7.5/9
North	$1.5^{+0.5}_{-0.3}$	$0.74^{+0.09}_{-0.07}$	-	-	$1.58 \pm 0.15$	17.2/18
	$1.4^{+0.5}_{-0.4}$	$0.69^{+0.10}_{-0.07}$	$8.1^{+1.8}_{-0.4}$	$\sim 4.8$	$1.66 \pm 0.13$	17.9/17
East-west	$1.3 \pm 0.2$	$0.80^{+0.09}_{-0.07}$	-	-	$1.68 \pm 0.10$	18.9/13
	$1.1 \pm 0.2$	$0.73^{+0.08}_{-0.07}$	$6.3 \pm 0.6$	$\sim 4.0$	$1.70 \pm 0.09$	16.6/12
All	$1.29^{+0.29}_{-0.08}$	$0.77^{+0.04}_{-0.02}$	-	-	$1.75 \pm 0.04$	18.2/24
	$1.11^{+0.18}_{-0.15}$	$0.71^{+0.03}_{-0.04}$	$7.7 \pm 0.4$	$\sim 2.7$	$1.71 \pm 0.03$	15.4/23

note: The  $\beta$ -model fits to the 0.5 - 1.5 keV  $S_X$  in different directions (truncated or not). The local PSF is included in the fits.  $f_{\text{back}}$  is the flux of the local background, which slightly decreases from the south (closer to the cluster center) to the north.

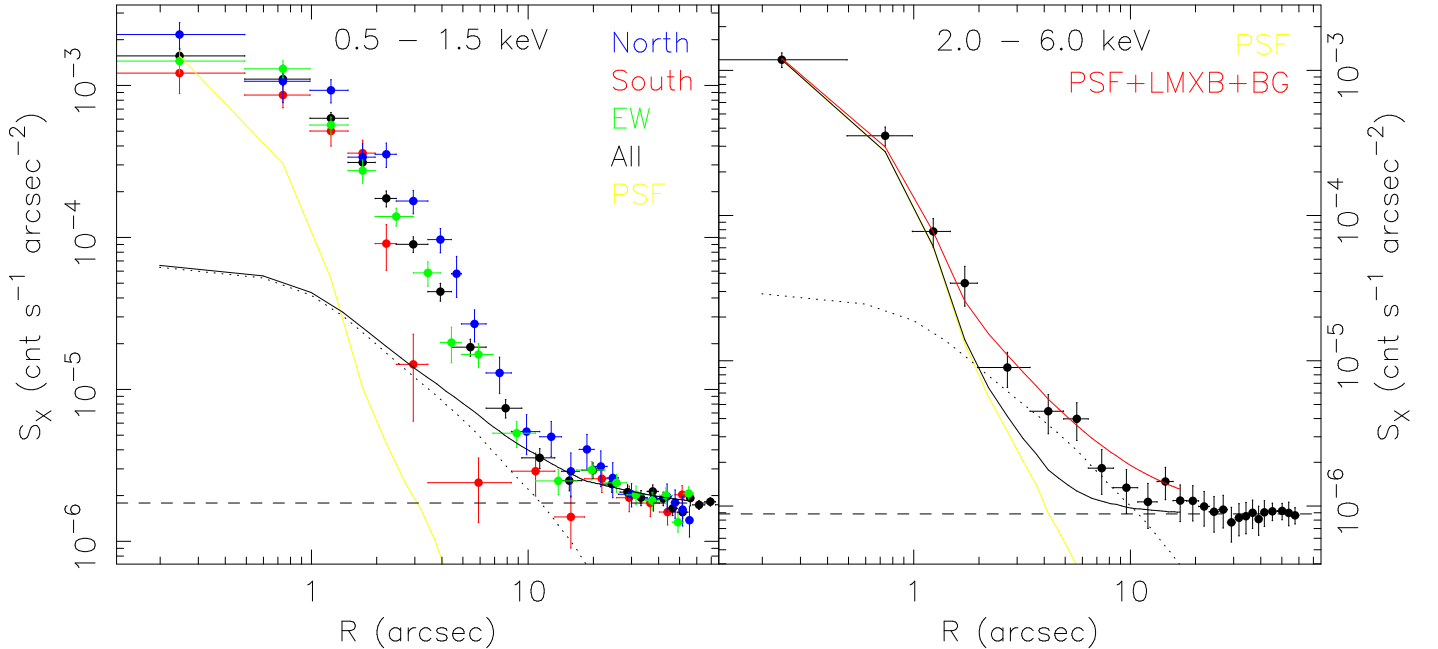


FIG. 2.— **Left:** the 0.5 - 1.5 keV surface brightness profiles centered on the NGC 1265 nucleus (black: azimuthally averaged; red: south; blue: north; green: east-west). The north region is from azimuthal angle  $42^\circ$  to  $135^\circ$  (measured from the west), while the south region is from azimuthal angle  $227^\circ$  to  $309^\circ$ . The east-west region includes all azimuthal angles left. The yellow line represents the local 0.5 - 1.5 keV PSF. The dashed line represents the background determined from the azimuthally averaged profile between  $30''$  and  $120''$ . The dotted line is the optical light profile determined from the *HST* observations and is normalized to match the predicted LMXB luminosity from the scaling relation by Sarazin et al. (2001), with the assumption that the LMXB distribution follows the optical light. The solid line is the sum of the previous two components. The southern surface brightness profile shows a sharp edge at  $\sim 3''$  (smoothed by the PSF) from the nucleus, while the extension in the north can be traced to at least  $8''$  (excluding the possible LMXB component). **Right:** the 2 - 6 keV surface brightness profile. The yellow line, dashed line and the dotted line represent the same components as those in the left panel, but in the 2 - 6 keV band. The black solid line is the sum of the PSF and the local background, which clearly underestimates the data from  $2''$  to  $8''$ . The red line is the sum of the PSF, the local background and the LMXB component scaled from the optical light, which roughly reproduces the data.

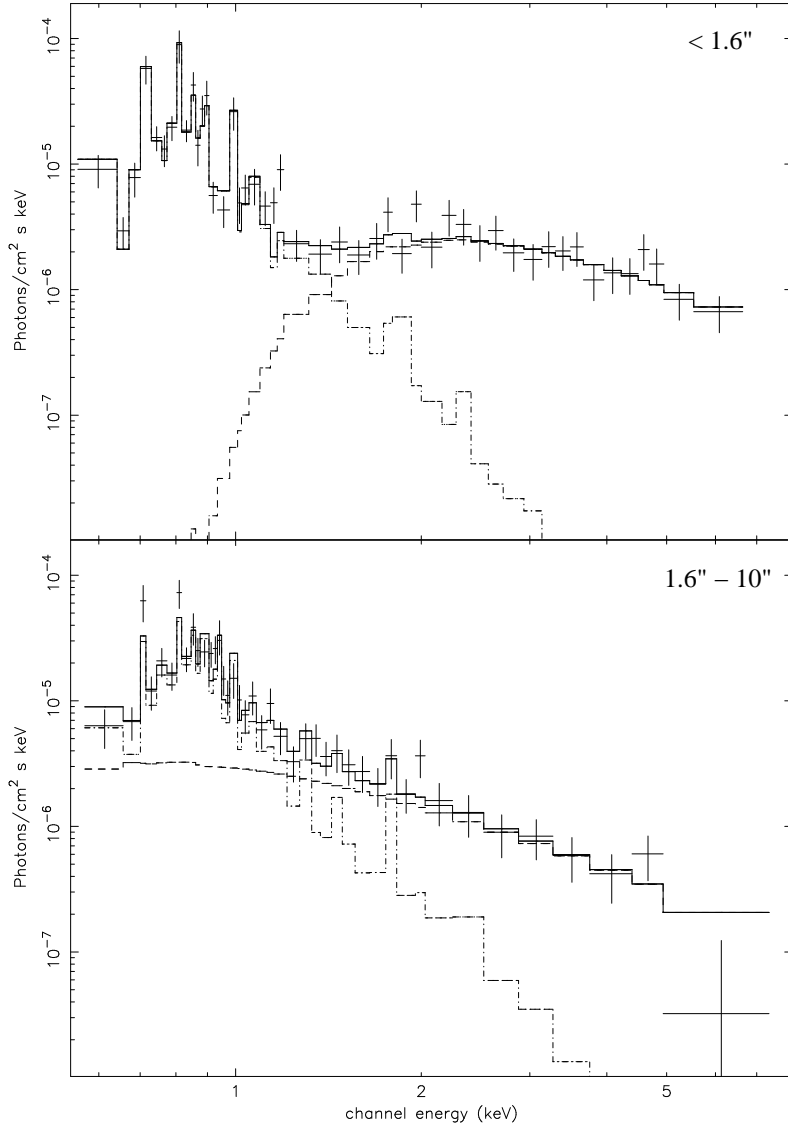


FIG. 3.— The spectra of the inner ( $< 1.6''$ ) and outer ( $1.6'' - 10''$ ) regions of the NGC 1265 X-ray source, with the two-component models shown as the fourth and the seventh rows in Table 1 (dot-dash line: corona emission; dashed line: absorbed nuclear emission or LMXB emission; solid line: the sum). The blend of iron L lines is significant in both spectra. The shapes of the spectra at  $E > 1.5$  keV are different. The absorbed nucleus dominates in the hard X-rays for the inner region, while the LMXB is a significant component for the outer region.

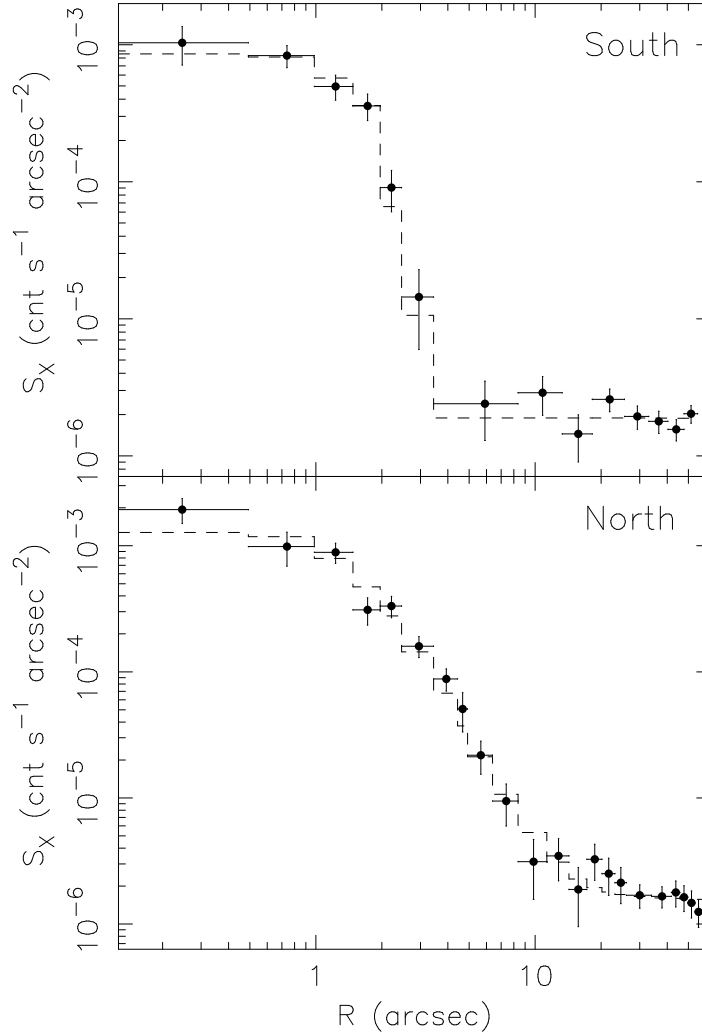


FIG. 4.— **Upper:** the 0.5 - 1.5 keV surface brightness profile of the south sector with the best-fit model, a truncated  $\beta$  model with a constant background. The estimated nuclear emission at the 0.5 - 1.5 keV band is subtracted from the profile. The best-fit model has been convolved with the local PSF, which smoothes the sharp edge. The surface brightness jump across the edge is  $\sim 106$ . **Lower:** the 0.5 - 1.5 keV surface brightness profile of the north sector with the best-fit model, a  $\beta$  model with a constant background. The estimated nuclear emission and the LMXB emission is subtracted from the profile. The best-fit model has been convolved with the local PSF. The truncation of the  $\beta$  model is not significant. Despite the not so small errors, the gas distributions of these two sectors are consistent with the same one, but with different truncation radii (Table 2).